# Comparison of Satellite-Based InSAR methods for Monitoring Geothermal Areas at Rotokawa: PS versus SBAS

Mark Harvey[1] and Jim McLeod[2]

[1]Harvey Geoscience Ltd, 51 Gifford Rd, West Hartford, CT 06119, USA

[2]Waikato Regional Council, Private Bag 3038, Waikato Mail Centre, Hamilton 3240

mark@harveygeoscience.com

**Keywords:** *Rotokawa, Zealand, StaMPS, SBAS, geothermal, subsidence, InSAR, Sentinel.*

## ABSTRACT

This study utilises freely available Sentinel-1 satellite InSAR data to map surface deformation at the Rotokawa thermal area between 2014 - 2024. Three InSAR methods are used to examine the area: PS InSAR (StaMPS), and two SBAS methods (GMTSAR and LiCSBAS). While StaMPS provides the best resolution to localised deformation, both SBAS methods have the advantage of providing total coverage across the survey area. LiCSBAS can efficiently process very long time series (i.e. 10 years) and may be applied to very large areas (> 1000 km$^2$). A disadvantage of LiCSBAS is that it may not resolve localised areas of surface deformation, e.g. small subsidence bowls (< 200 m radius). This is a limitation of the method, which utilises a coarser grid and averages signals over a wider area.

## 1. INTRODUCTION

Waikato Regional Council (WRC) previously conducted surface change analysis in the Taupo Volcanic Zone (TVZ) using Sentinel-1 satellite synthetic aperture radar (SAR) data (Harvey et al., 2022, Harvey et al., 2019). The analyses used the Stanford Method for Persistent Scatterers (StaMPS), and results showed good agreement with traditional levelling surveys, particularly in areas with infrastructure and bare thermal ground. Here we explore the use of freely available Sentinel-1 satellite InSAR data to focus on surface deformation at the Rotokawa thermal area nearby Lake Rotokawa (Figure 1). A key objective is to determine how StaMPS compares to SBAS, an alternate InSAR method.

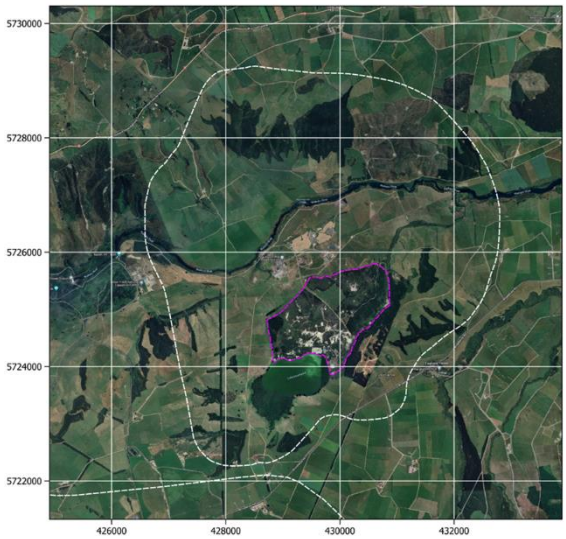


**Figure 1: Rotokawa geothermal system. Note: Magenta boundary shows thermal ground study area.**

## 2. METHODS

### 2.1 StaMPS and SBAS background

This study compares three InSAR approaches, StaMPS (Hooper, 2008), and two Small Baseline Subset (SBAS) methods: GMTSAR (Sandwell et al., 2011) and LiCSBAS (Morishita et al., 2020). All are satellite-based multi-temporal methods for the measurement of gradual ground deformation, often associated with geothermal activity.

StaMPS uses reflected satellite radar signals to accurately measure ground displacement. The method relies upon a "stack" of satellite images collected over time to identify persistent scatterers (PS). PS are surface objects that reflect radar, including bare thermal ground, infrastructure, large rock outcrops, and other prominent natural features. Using this method, the motion of each PS can be precisely measured, and ground deformation can be determined.

Like StaMPS, SBAS methods also utilise a stack of satellite radar images, but these are processed using a different algorithm; unlike StaMPS, which relies heavily on point-like PS, SBAS can utilise distributed scatterers (DS) which are broader areas of radar scatter. DS may provide better coverage in vegetated areas with little to no PS. A potential limitation of SBAS is in the averaging of signals from a wider area; extreme values may be smoothed over or "averaged out".

Further details are available for GMTSAR (Sandwell et al., 2011) and LiCSBAS (Morishita et al., 2020).

### 2.2 Post-processing workflow

For both StaMPS and GMTSAR, mean annual velocity estimates are derived from time series of elevations recorded over a 2-year period of observation (2022 to 2024). The velocity estimate is based on a linear regression through the series. Controlled experiments show InSAR derived velocities are usually consistent (± 1 mm/yr) with conventional GNSS (Cigna et al., 2021).

Satellite data with line-of-site (LOS) viewing geometry from ascending and descending orbits (orbit passes 81 and 73 respectively) are combined to provide an estimate of vertical deformation. Further details of the method used to derive vertical motion are provided in Manzo et al. (2006).

For StaMPS processing, all motions are relative to the Aratiatia Dam (424900, 5725300) located outside the system boundary. This area is chosen for consistency with prior levelling programs for Wairakei-Tauhara and Rotokawa that utilise this location as the network origin (Bromley et al., 2015).

For GMTSAR, motion is relative to the average motion of DS within an ~ 64 km$^2$ area centred on the Rotokawa

geothermal system, which is assumed to be zero (no processing parameter was available to specify a reference area).

Aratiatia Dam was flagged by LiCSBAS as being an unsuitable reference area (low coherence), so an alternate location was chosen in the Taupo township (421000, 5717000); historical levelling surveys show this location is stable with respect to the Aratiatia Dam (Bromley et al., 2015). A longer (10-year) time series was processed (2014 - 2024) to take advantage of the computationally less-intensive workflow offered by LiCSBAS.

Table 1 provides a summary of datasets included in the processing. All coordinates UTM WGS84.

**Table 1: InSAR processing stacks**

| Orbit Pass | Stack Size | First Image | Last Image | Master Image | Method |
|---|---|---|---|---|---|
| 73 | 55 | 6/6/22 | 2/5/24 | 13/06/23 | PS/GMTSAR |
| 81 | 58 | 7/6/22 | 3/5/24 | 15/04/23 | PS/GMTSAR |
| 73 | 55 | 22/10/14 | 2/5/24 | na | LiCSBAS |
| 81 | 58 | 4/11/14 | 4/1/24 | na | LiCSBAS |

## 3. RESULTS

### 3.1 STAMPS (2022 – 2024)

PS point data is mapped for LOS velocities, for descending (Figure 2), and ascending (Figure 3) orbit datasets. Vertical velocities are mapped (Figure 4).

### 3.2 GMTSAR SBAS (2022 – 2024)

DS point data is mapped for LOS velocities, for descending (Figure 5), and ascending (Figure 6) orbit datasets. Vertical velocities are mapped (Figure 7).

### 3.3 LICSBAS (2014 – 2024)

10-year average (2014 – 2024) vertical velocities are mapped (Figure 8).

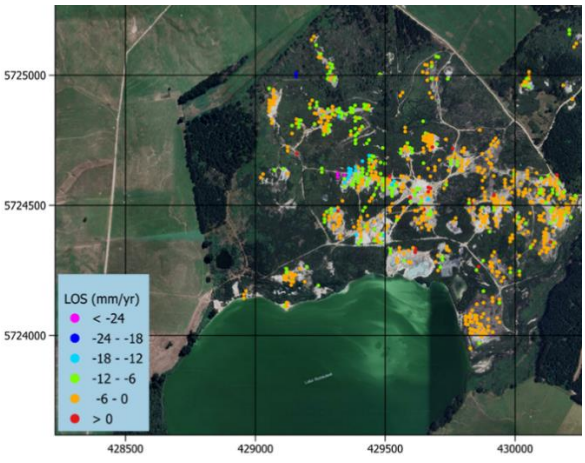


**Figure 2: Mean annual motion for PS, June 2022 – May 2024, descending orbit 73.**

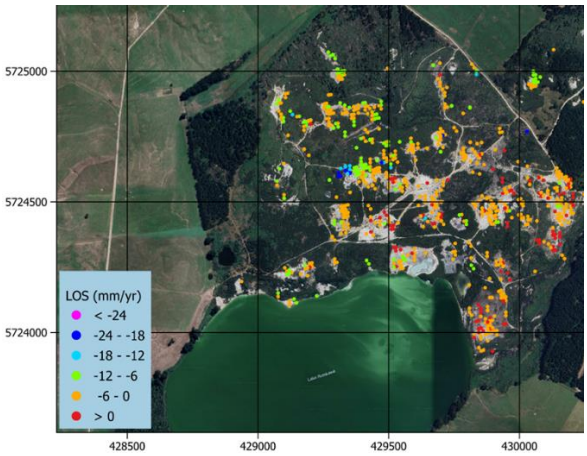


**Figure 3: Mean annual motion for PS, June 2022 – May 2024, ascending orbit 73.**

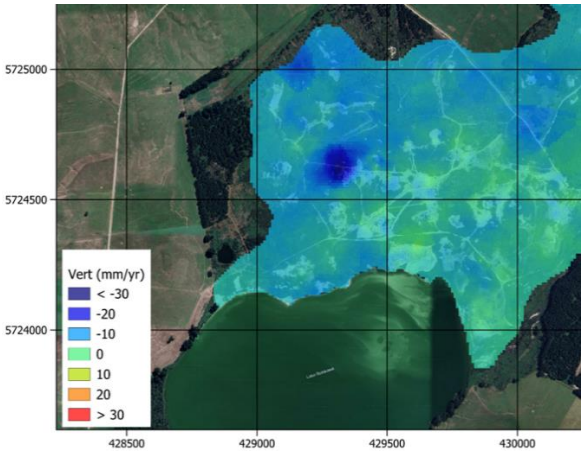


**Figure 4: Vertical deformation (StaMPS) InSAR June 2022 – May 2024.**

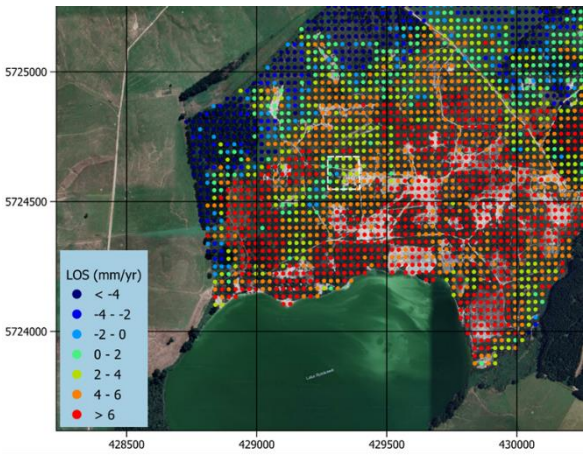


**Figure 5: Mean annual motion for GMTSAR DS (SBAS), June 2022 – May 2024, descending orbit 73. White box shows the location of the subsidence bowl visible in StaMPS results (Figure 4).**

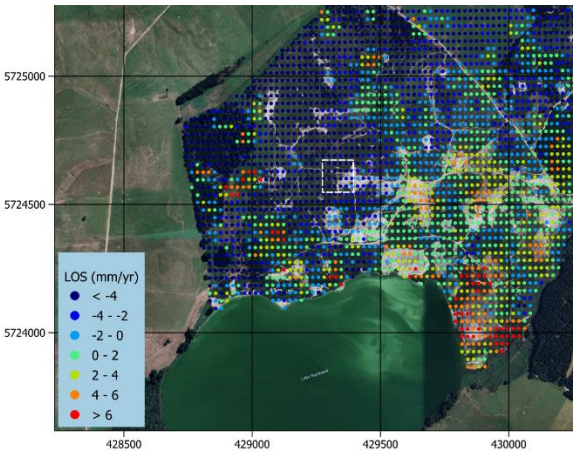


**Figure 6: Mean annual motion for GMTSAR DS (SBAS), June 2022 – May 2024, ascending orbit 73. White box shows the location of the subsidence bowl visible in StaMPS results (Figure 4).**

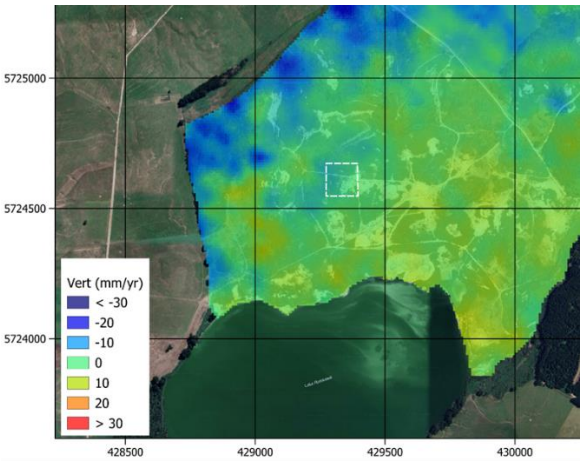


**Figure 7: Vertical deformation GMTSAR SBAS InSAR June 2022 – May 2024. White box shows the location of the subsidence bowl visible in StaMPS results (Figure 4).**

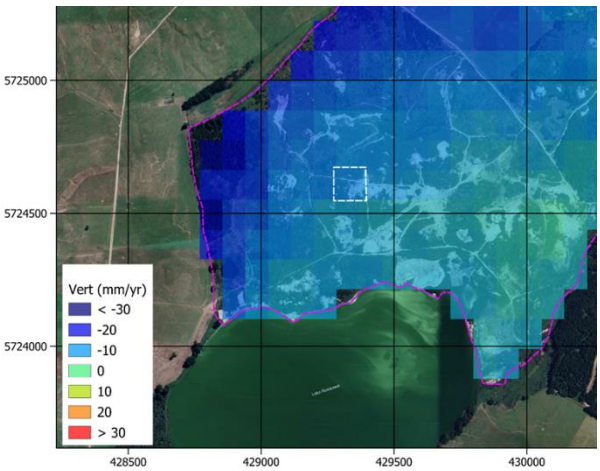


**Figure 8: Vertical deformation LiCSBAS InSAR 2014 – May 2024. White box shows the location of the subsidence bowl visible in StaMPS results (Figure 4).**

## 4. DISCUSSION

### 4.1 Overview

The StaMPS-derived vertical motion map (2022 – 2024) shows weak subsidence (< 5 mm/year) across the central Rotokawa thermal area, with greater rates at the western and northern periphery (Figure 4), and a subsidence bowl in the west (maximum rate at bowl centre -29 ± 2 mm/yr). However, PS are scarce in the bowl area (Figure 2 and Figure 3), so it is possible the bowl is an artifact of interpolation.

For GMTSAR (2022 – 2024), the DS map for ascending orbit 81 shows a circular subsidence area that supports the existence of the bowl (Figure 6), but descending orbit 73 is inconclusive (Figure 5). The vertical motion map shows weak inflation (< 5 mm/year) across the central Rotokawa thermal area, and only slight subsidence at the bowl area (maximum rate 4 ± 0.7 mm/yr) (Figure 7). As with StaMPS results, greater rates of subsidence occur at the western and northern periphery.

The LiCSBAS vertical map (2014 – 2024) shows a gradation of subsidence across the study area from -28 mm/year in the west to -3 mm/year in the east (Figure 8). No subsidence bowl is evident.

### 4.2 StaMPS versus SBAS

Comparison of point maps illustrates the complete coverage of GMTSAR (Figure 5 & Figure 6) versus StaMPS (Figure 2 & Figure 3); large areas of the StaMPS results have few PS because of vegetation.

LiCSBAS results do not show the subsidence bowl (Figure 8), but this may result from the lower resolution of the method (100 m pixel) and/or the different observation period (2014 - 2024). The limited resolution of LiCSBAS is a disadvantage that is offset by its ability to efficiently handle much longer time series (e.g. 10 years) and larger areas than either StaMPS or GMTSAR; LiCSBAS is well suited to long duration and/or regional scale ground deformation studies, but less suited to the study of smaller-scale phenomenon. By comparison, time series for StaMPS and GMTSAR are limited here to a 24-month duration (Table 1). For StaMPS, longer stacks are possible but would produce even lower PS density. Longer GMTSAR stacks are also possible, but processing would require greater computational resources.

### 4.3 StaMPS Time Series at Subsidence bowl (2022 – 2024)

Time series are plotted for StaMPS descending (Figure 9A) and ascending PS (Figure 9B) selected from the centre of the subsidence bowl area. Both series are linear over the 2-year observation period ($r^2 > 0.8$).

Long term (10 year) time series are shown for LiCSBAS descending DS selected from the centre of the subsidence bowl area (Figure 9C). Series are strongly linear over the 2-year observation period ($r^2 > 0.94$) showing the continuous nature of subsidence in the area.

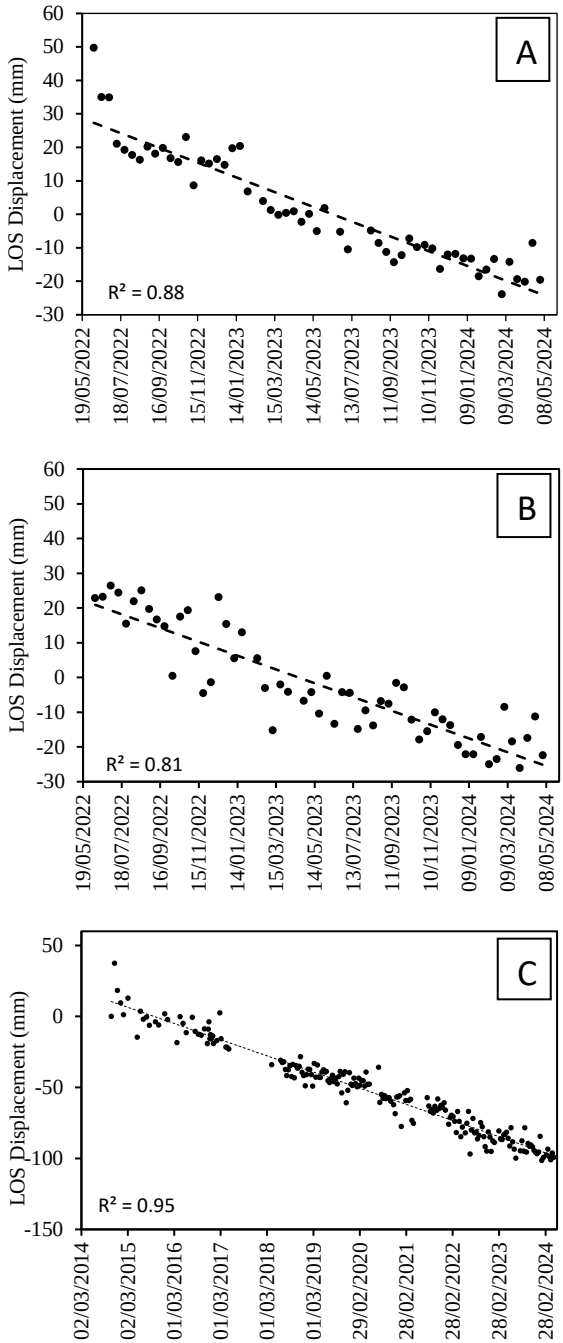


**Figure 9: Time series at Rotokawa subsidence bowl: (A) PS descending orbit 73, (B) PS ascending orbit 81, and (C) LiCSBAS descending orbit 73.**

### 4.3 Subsidence Bowl: Depth and Volume for Source Process

Mean vertical subsidence rates based on StaMPS InSAR are used to invert for depth and rate of volume loss at the Rotokawa bowl (Mogi, 1958). A Monte-Carlo simulation (10,000 realisations) minimised square misfit between observed and calculated displacements along a 175 m profile of the StaMPS vertical motion surface (Figure 10). Results provide estimates of depth (98 m) and the rate of volume loss (1052 $m^3$/year) for the subsidence source.

The exact cause of subsidence may be localised compaction of reservoir rock due to pore pressure decline and/or thermal contraction due to cooling of the reservoir rocks. Reservoir rock may be cooled by natural recharge, or by water vaporization, where heat is transferred from rock to fluid in a steam cap.

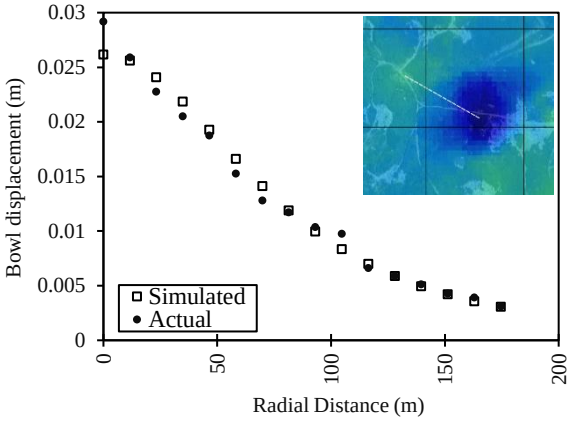


**Figure 10: Mogi model of the Rotokawa subsidence bowl based on StaMPS InSAR vertical motion. Note: map inset, white dash line shows curve profile.**

### 4. CONCLUSIONS

This study utilises freely available Sentinel-1 satellite InSAR data to map surface deformation at the Rotokawa thermal area between 2014 and 2024. Three InSAR methods are used to examine the area: PS InSAR (StaMPS), and two SBAS methods (GMTSAR and LiCSBAS).

SBAS can complement StaMPS in vegetated areas, i.e. where fewer PS exist. SBAS is evaluated here to potentially improve StaMPS coverage where vegetation may cause temporal and spatial decorrelation of the radar signal.

Results show both SBAS methods have the advantage of providing total coverage across the survey area, while LiCSBAS can efficiently process very long time series (i.e. 10 years) and may be applied to very large areas (> 1000 $km^2$).

A disadvantage of LiCSBAS is that it may not resolve localised areas of surface deformation, e.g. small subsidence bowls (< 200 m radius). This is a limitation of the method, which utilises a coarser grid and averages signals over a wider area.

In summary, while StaMPS and GMTSAR can be combined for the purpose of monitoring small or medium sized areas, LiCSBAS is better suited to long-duration and/or regional scale ground deformation studies. Of the three methods, StaMPS provides the best sensitivity to localised, extreme rates of deformation.

**REFERENCES**


Cigna, F., Esquivel Ramírez, R., & Tapete, D. (2021). Accuracy of Sentinel-1 PSI and SBAS InSAR Displacement Velocities against GNSS and Geodetic Levelling Monitoring Data. Remote Sensing, 13 (23), 4800.

Harvey, M.C., Luketina, K.M., McLeod, J., and Rowland J.V. (2019). Geothermal Subsidence and Inflation in Taupo: A Comparison of Detection Methods. Proceedings 40th New Zealand Geothermal Workshop.

Harvey, M.C., McLeod, J., and Calibugan, A. (2022). Recent Observations of Ground Deformation at TVZ Geothermal Systems Using Multi-Temporal InSAR. Proceedings 44th New Zealand Geothermal Workshop.

Hooper, A. (2008). A multi-temporal InSAR method incorporating both persistent scatterer and small baseline approaches, Geophysical Research Letters, 35, L16, 302.

Manzo, M., Ricciardi, G. P., Casu, F., Ventura, G., Zeni, G., Borgström, S., and Lanari, R. (2006). Surface deformation analysis in the Ischia Island (Italy) based on spaceborne radar interferometry. Journal of Volcanology and Geothermal Research, 151(4), 399-416.

Morishita, Y., Lazecky, M., Wright, T. J., Weiss, J. R., Elliott, J. R., and Hooper, A. (2020). LiCSBAS: An open-source InSAR time series analysis package integrated with the LiCSAR automated Sentinel-1 InSAR processor. Remote Sensing, 12(3), 424.

Mogi, K. (1958). Relations between the eruptions of various volcanoes and the deformations of the ground surfaces around them. Bulletin of the Earthquake Research Institute. 239:352–367.

Sandwell, D., Mellors, R., Tong, X., Wei, M., & Wessel, P. (2011). Open radar interferometry software for mapping surface Deformation. EOS Transactions, 92(28), 234-234.